Structural and energetic properties of vacancy defects in MXene surfaces

José D. Gouveia [*] and José R. B. Gomes [†]

CICECO – Aveiro Institute of Materials, Department of Chemistry, University of Aveiro, Campus Universitário de Santiago, Aveiro, Portugal

(Received 29 November 2021; accepted 11 February 2022; published 28 February 2022)

Density functional theory calculations were employed to investigate the structure and energetics of vacancy defects on 84 MXene surfaces, composed of different M (Ti, Zr, Hf, V, Nb, Ta, Cr, Mo, or W), X (carbon or nitrogen), T (oxygen of fluorine), and atomic layer stacking (ABC or ABA) combinations. Structurally, we found that, in most cases, the effect of the presence of the vacancy on the surrounding atoms is to push them away from the vacant site due to the missing screening charge and the reinforcement of the remaining interatomic bonds. The reconstruction energy associated to this surface relaxation was found to range from a few tenths of eV to a few eV. On the bare ABC-stacked carbide MXenes, we found M and X vacancy formation energies between 2 and 3 eV. On nitrides, M vacancy formation energies are decreased, while X ones seem to increase. By terminating the MXenes with an O layer, M formation energies are significantly increased, reaching over 9 eV in some cases, in agreement with theoretical and experimental results of the literature, whereas X vacancy formation energies become smaller. The F termination was found to have the same effect as O on X vacancy formation energies with respect to clean MXenes, but to decrease M vacancy formation energies. The F termination allows more easily created M and N vacancies than the O termination. The creation of vacancies on some ABC-stacked M_2XF_2 MXenes led to extreme lattice deformation which suggests that the experimental synthesis of M_2NF_2 with metals from groups 5 and 6 of the Periodic Table, and M_2CF_2 with metals from group 6, through etching using a hydrogen fluoride aqueous solution [HF (aq)] will lead to ABA-stacked MXenes. The formation energies of the MT double vacancies were found to correlate approximately linearly with the sum of the corresponding M and T single-atom vacancy formation energies. All MXenes studied in this work fit in the same correlation line, implying that one can predict the formation energy of double vacancies on MXenes, made of any M, X, and T elements, and with atomic layers stacked in an ABC or ABA fashion, if the formation energies of the corresponding single vacancies are known. The method used by theoretical works, such as this one, to calculate formation energies has two crucial limitations: the values thus obtained depend on the chosen single-atom energy references, and kinetic effects such as energy barriers are not included. Here, we cautiously discuss these limitations, compare formation energies calculated using different energy references, and propose mechanisms for the formation of vacancies that include atomic migration barriers.

DOI: 10.1103/PhysRevMaterials.6.024004

I. INTRODUCTION

It has now been around ten years since MXenes joined the large family of two-dimensional (2D) materials [1]. With a name inspired by that of graphene, MXenes are typically made up of a few $(n + 1)$ layers of atoms of an early transition metal element (M) intercalated by n layers of carbon or nitrogen (X). Upon synthesis, the metallic layer is very reactive, and the MXene becomes terminated by a layer whose composition depends on the synthesis method. The first synthesis method consisted of using an aqueous solution of hydrogen fluoride [HF (aq)] to selectively etch out the A element from the Ti_3AlC_2 MAX phase [2]. This resulted in a $Ti_3C_2T_x$ MXene terminated by $T_x = F$, O or OH layers. Synthesis methods which do not rely on HF (aq) can result in MXenes with only O and OH terminations [3], and postsynthesis heating treatments can eliminate the surface termination completely [4,5]. The general stoichiometry of MXenes is therefore $M_{n+1}X_nT_x$, with $n = 1$–5, and with O being the most popular termination. Since the discovery of the first MXene, over 30 different MXenes have been experimentally realized to date, including some which mix metallic elements, and as thick as the bimetallic $Mo_4VC_4T_x$ [6]. Theoretically, over a hundred MXenes have been predicted due to the countless possible combinations of M, X, and T elements, stoichiometries, and even atomic layer arrangements [7]. For this reason, despite being a decade old, the field of MXenes still has plenty of room for growth.

The general properties of MXenes include high electrical and metallic conductivities, hydrophilicity, very large surface area, and a huge variety of tunable structures and compositions. The fact that MXenes can be produced by utilizing HF (aq) shows they survive harsh conditions and highly corrosive environments. The V_2CT_x MXene, for instance, was demonstrated to be stable in inert, oxidizing, and reducing environments [8], and the $Ti_3C_2T_x$ MXene was shown to resist temperatures up to 900 °C and a pressure of 26.7 GPa [9,10]. MXenes find application in areas such as ecofriendly

[*]Corresponding author: gouveia@ua.pt
[†]Corresponding author: jrgomes@ua.pt

energy, water purification, or catalysis [5,11,12]. In particular, Mo_2CT_x was synthesized by removing Ga from the Mo_2Ga_2C MAX phase using HF (aq) [5], yielding an MXene whose surface was terminated by around 70% F and 30% O. This surface was then used as catalyst for the water-gas shift (WGS) reaction, a process crucial for the hydrogen economy, with Mo_2CT_x showing high stability and selectivity towards the desired products in the conditions under which the reaction was conducted.

While pristine (without T_x terminations) MXenes have been produced, they are prone to oxidation, which hampers wide application in catalysis. On the one hand, clean MXenes are very reactive towards all kinds of chemical compounds, and easily dissociate even molecules with strong bonds such as nitrogen [13]. The problem is that the adsorption of both reagents and products is so strong that the catalyst regeneration via product desorption is very energy consuming. On the other hand, O-terminated MXenes, which are the most common ones, are often not able to activate available surface reacting species, instead being more suited for sensing applications [14–16]. Thus, the F termination presents itself as very suitable for catalytic applications, since it allows moderate molecule adsorption strength, while avoiding the highly oxophilic surface from becoming covered by O and less active for catalysis [5]. This effectively and realistically encourages the use of MXenes as catalysts. Implantation of MXene surfaces with atoms of less oxophilic metallic elements is another way to improve the catalytic activity. Single-atom catalysts (SACs) can be deposited on MXenes on interstitial sites [17] or on substitutional sites [18]. As an example of the latter, the Pt-based SAC $Pt@Ti_3C_2T_x$ was experimentally and theoretically shown to display adsorption and activation energies suitable for catalysis of the formylation of amines, displaying very high conversion rates and selectivity and a turnover number higher than that of Pt nanoparticles [18]. The Pt atoms were deposited on vacant sites of the MXene, previously occupied by Ti. Another theoretical study tested the activity of several SAC on oxygen vacancies in V_2CO_2 and predicted that a Zn SAC should successfully catalyze CO oxidation with a very low energy barrier [19]. A very recent computational study compared the activity of 16 transition metal single atoms on the V_2CO_2 MXene, as catalysts of the oxygen reduction and hydrogen oxidation reactions, and found that different metallic elements exhibit higher catalytic activity depending on whether they occupy an interstitial or an O-vacancy site [20].

The possibilities described in the previous paragraph have driven the study of single vacancies and vacancy clusters in MXenes. Emphasis has been given to Ti_2CO_2, on which the Ti, C, and O single vacancies have been studied, with the carbon vacancy (V_C) having the lowest formation energy, and the Ti vacancy (V_{Ti}) the highest one [21,22]. The values of the formation energies vary between different studies, mainly due to the different ways to calculate the energy of a single atom, but all studies agree that a metal vacancy (V_M) is energetically the costliest to create, while vacancies resulting from the removal of X = C, N are the cheapest ones. One last noteworthy possibility is the creation of MT double vacancies to accommodate the SAC, as has been done for realizing the hydrogen evolution reaction on $Pt@Mo_2TiCT_x$ [23].

In this work, we perform a systematic first-principles study of the structural and energetic properties of four kinds of vacancies on MXene surfaces composed of nine different M elements and investigate how these properties vary with the M and X elements, the surface termination, and the atomic layer stacking of the MXene. In the following, we describe the computational method, followed by a presentation of the results, and a summary of the conclusions. The Supplemental Material [24] includes additional tables and figures with formation and reconstruction energies that complement the discussion in the main text.

II. COMPUTATIONAL METHODS

All of the first-principles calculations were performed with the VASP package [25–28], using the Perdew-Burke-Ernzerhof (PBE) exchange-correlation functional [29]. The interactions between core electrons and valence ones were implicitly treated by the projector augmented wave (PAW) method [30]. The Kohn-Sham equation was solved by expanding the wave function of valence electrons as plane waves with an energy cutoff of 415 eV for supercell calculations and of 550 eV for unit cell optimizations. Atomic position relaxation stopped when the forces acting on each atom became lower than 0.005 eV/Å and the total energies were converged within 10^{-6} eV. The Brillouin zone was sampled using Γ-centered grids of k points, which are more adequate for the employed cell shape [31]. Grids of $11\times11\times1$ and $3\times3\times1$ k points were used for unit cell and supercell calculations, respectively. Our preliminary tests, with denser k-point grids, higher energy cutoffs, and tighter convergence criteria, showed that the parameters described yield defect formation energies converged within 3 meV, and that spin polarization has no effect on the structure or energetics of the studied systems. To avoid periodic interference in the direction perpendicular to the surfaces, the simulation boxes contained approximately 20 Å of vacuum height.

The metallic elements considered form a 3×3 square in the Periodic Table of the Elements, namely, Ti, Zr, Hf, V, Nb, Ta, Cr, Mo, and W, also considered in our previous studies with MXenes [7,13,32]. For each of these, we began by constructing and optimizing a unit cell of the corresponding M_2XT_2 MXene. The lattice constants obtained here after unit cell optimization are in very good agreement with the ones found in the literature. For example, the lattice constant of 3.03 Å calculated for Ti_2CO_2 is within 1% of the one in Refs. [21,33] (3.04 Å), calculated by two other research groups at the same level of theory. The same quantity calculated for Ti_2CF_2, 3.06 Å, again agrees with the corresponding values found in the same references (3.06 and 3.04 Å, respectively). The unit cells of the bare and terminated MXenes are made up of three and five atomic layers, M-X-M and T-M-X-M-T, respectively, but the most stable way these atomic layers stack depends on the M and X elements. On the one hand, MXenes made of metals of group 4 (Ti, Zr, Hf) or group 6 (Cr, Mo, W) of the Periodic Table always stack in an ABC or ABA fashion (see Fig. 1), respectively [7]. On the other hand, group 5 (V, Nb, Ta) MXenes can prefer either termination depending on the X and T elements [7]. For ABC MXenes, the atoms of the two M layers and the X layer are all misaligned with

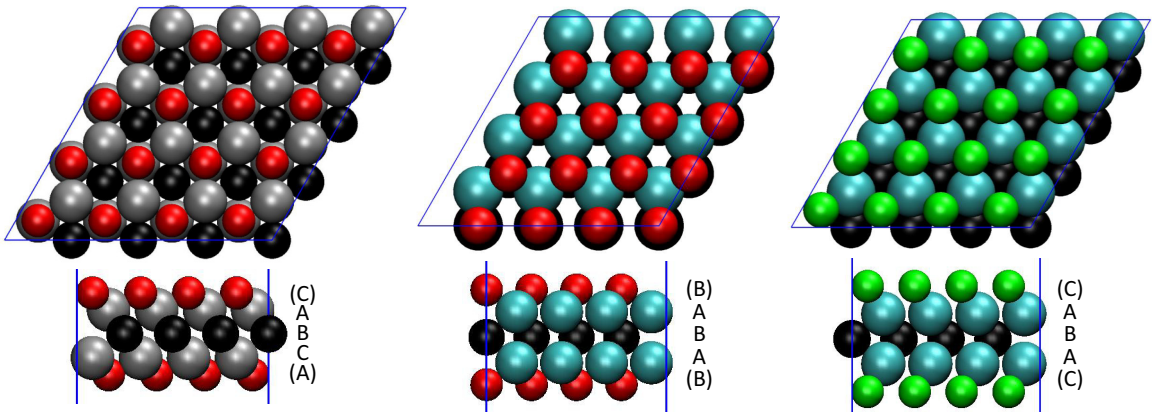

FIG. 1. Top (top images) and side (bottom images) views of MXene $p(4 \times 4)$ supercells. On the left, the Ti_2CO_2 MXene is shown, as an example of an MXene that displays ABC atomic layer stacking, and whose O surface termination aligns with the farthest metal layer, as displayed by the letters ABC next to the side view (letters in parentheses refer to the alignment of the termination layer). At the center and on the right, the Mo_2C MXene is shown, terminated by O and F, respectively, and displaying ABA atomic layer stacking, seen by the vertical alignment of its two metal layers, and identified by the letters ABA next to the side view. Color code for spheres: C in black, O in red, Ti in grey, Mo in blue, and F in green.

respect to each other (with trigonal D_{3d} symmetry; see Fig. 1), and the T layer, O or F, is aligned with the farthest M layer, for an overall C-A-B-C-A stacking. However, on the ABA MXenes, the two metal layers are aligned with each other (resulting in hexagonal close-packed D_{3h} symmetry), and the alignment of the T layer depends on its composition and the M element. This alternative preferred alignment has been known at least since 2016 to be the most stable one for the Mo_2C MXene [34]. Further evidence of the existence of MXenes with ABA atomic layer stacking was later found when the surfaces of the (ABC) Mo_2N and W_2N MXenes were theoretically predicted to distort upon N_2 adsorption [35], in what can be regarded as an attempt by the system to transition to its most stable ABA stacking, allowed by the symmetry breaking caused by the adsorption. When V_2N and Mo_2N MXene surfaces were first experimentally synthesized from V_2C and Mo_2C, using an ammoniation process to replace C atoms by N ones, the Mo_2N sample was described as having a distorted structure with hexagonal close-packed symmetry [36], representing additional indication of the occurrence of ABA stacking. Regardless of stacking, the atoms of each layer of any given MXene are placed at the vertices of equilateral triangles (as seen in Fig. 1), and spaced by around 3 Å, the typical lattice constant of these surfaces. For this reason, atoms of the X layer (C or N) are not bonded to each other and phenomena equivalent to the Stone-Wales defects should not occur. Nevertheless, we verified this by introducing this defect (rotation of one C-C "bond" by 90° around an axis perpendicular to the surface) on a Ti_2C MXene surface. After relaxation of the atomic positions, we observed that the two C atoms had returned to their original positions, revealing that this defect is not stable.

The defect-free MXene surfaces were modeled as rhombic supercells with periodic boundaries in all Cartesian directions, containing $p(4 \times 4)$ MXene unit cells (80 atoms), to avoid interaction between point defects and their adjacent periodic copies (see Fig. 1). The vacancy defects were introduced by deleting the respective atom(s) from the optimized supercell and allowing the system to relax the atomic positions again. The defect formation energy was then calculated as

$$E_{\text{form}} = E_{\text{defect}} + E_{\text{atom}} - E_{\text{MXene}},$$

where E_{defect} is the total calculated energy of the reoptimized defective MXene surface, E_{MXene} is the energy of the pristine M_2XT_2 surface, and E_{atom} is the energy of the atom(s) removed to create the vacancy. In the case of metal vacancies, E_{atom} was the energy per atom of one unit cell of the bulk metal in its most commonly occurring form, i.e., a hexagonal-close-packed (hcp) solid for Ti, Zr, and Hf, and a body-centered-cubic (bcc) structure for the remaining six metals. The energy of a carbon atom was calculated as the energy per atom of one unit cell of diamond, the energy of an oxygen or nitrogen atom is half the energy of O_2 or N_2, respectively, and the energy of a fluorine atom is calculated from that of gaseous hydrogen fluoride (HF) and gaseous hydrogen (H_2) via $E_F = E_{HF} - \frac{1}{2}E_{H_2}$. Note that we chose this method of calculation of the energy of an F atom because the F surface termination that arises on MXenes is due to the application of HF (aq) to remove the A element from the MAX phase. Alternatively, one can compute it as $\frac{1}{2}E_{F_2}$, as it has been done in the literature. Below, we compare the results with both methods of calculation. The energy used as reference for the calculation of MT (T = O or F) double vacancies was simply the sum of the energy of one metal atom and one T atom, each calculated as described above.

At this point, we emphasize two critical details on the kind of information that formation energy values provide. First, the defect formation energies calculated in any theoretical work are not absolute and can vary by several eV, depending on the chosen method of calculation of single-atom energies. This dependency also implies that, in fact, one can only accurately compare E_{form} values of defects of the same type of atom, not of different atoms. For example, one can compare the E_{form} of a Ti vacancy on Ti_2C and Ti_2CO_2, because the single atom energy reference is the same. In contrast, comparing the E_{form} of a Ti with that of a C vacancy on Ti_2C is not rigorous, since changing the method of calculation of the Ti or the C atom could greatly affect the results. Second, formation energy

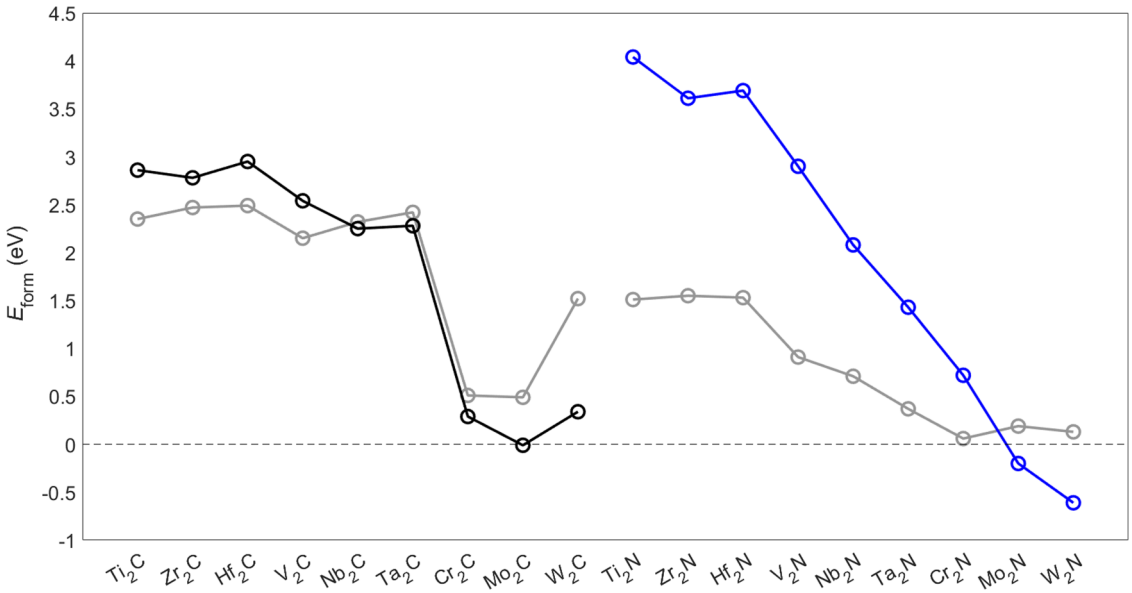

FIG. 2. Formation energies of vacancies in M_2X MXenes (values taken from Table S1 [24]). Carbides are shown on the left side, and nitrides on the right. The grey lines denote metal vacancies, and the black and blue lines denote carbon or nitrogen vacancies, respectively. The dashed line is placed at $E_{form} = 0$. Note that different reference species were considered in the calculation of E_{form} for different types of vacancies and direct comparison must consider this premise.

values calculated in this way only provide thermodynamic information, and do not include kinetic effects, such as energy barriers. As an example, one might calculate the formation energy of a V_N on W_2N and find negative value. Even disregarding the fact that the value thus found might be positive if a different energy of a single N atom had been chosen, it does not imply that N vacancies occur spontaneously on W_2N. Rather, it indicates that the process through which the N atom leaves the MXene surface towards another phase (such as N_2) is exothermic, but offers no information on the energy barrier that needs to be surmounted for the process to occur, namely for the N atom to cross the outer W layer. These critical aspects are often overlooked in theoretical studies and can mislead the reader.

Within our definition, negative formation energies reflect situations in which a system, composed of an incomplete MXene surface (due to the vacancy), and the missing atom in some other form, is thermodynamically more stable than the MXene crystal surface. As we will see, these are rare occurrences, a consequence of the stability of MXene surfaces when compared to other phases, and of the phases assumed for calculating the single-atom energies. In order to energetically quantify the structural deformation of MXene surfaces due to the presence of the vacancy defect, we calculated the *reconstruction energy*, which can be defined as the energetic difference between the M_2XT_2 surface with one of its atoms removed, after and before relaxation. Thus, by definition, all reconstruction energy values are negative, and higher absolute values are likely to be associated to defects whose presence induces more structural distortion. Calculated reconstruction energies are especially valuable for theoretical studies, as they can be directly compared to the corresponding ones in distinct theoretical or experimental works since, unlike formation energies, they do not depend on the method of calculation of single-atom energies.

III. RESULTS AND DISCUSSION

The presentation of the results is divided in four subsections. We first consider, in Sec. III A, the bare MXenes (i.e., MXenes without terminations), with the traditional ABC atomic layer stacking, and investigate the influence of the M and X elements on the structure and energetics of MXene vacancies. Then, we analyze the effect of the oxygen (Sec. III B) and fluorine (Sec. III C) surface terminations in tuning the properties of vacancies on MXenes. Last, in Sec. III D, we examine how these can be modified by considering an ABA layer stacking, which was suggested to be the most thermodynamically stable arrangement for carbide MXenes based on metal elements of group 6 of the Periodic Table, and for nitride MXenes based on elements of groups 5 and 6 [7].

A. MXenes without termination

Our base case was to consider all MXenes without any termination, i.e., with stoichiometry M_2X, and in the ABC stacking phase. The calculated vacancy formation energy values are plotted in Fig. 2, and the respective values are disclosed in the Supplemental Material Table S1 [24].

Let us first discuss the results for M_2C MXenes. The formation energy values of both V_M and V_C defects are clearly separated into two groups: one containing the MXenes made of metals from groups 4 and 5 of the Periodic Table, and another with the group 6 ones. On the M_2C MXenes of the first group, the formation energies are between 2 and 3 eV, while on the second group the formation energies are much lower. It is important to again highlight that the similarity between V_M and V_C formation energies occurs using what we considered as references for the energies of single atoms. For example, if instead of using diamond to obtain the energy of one C atom, one used graphene or another phase, the curve

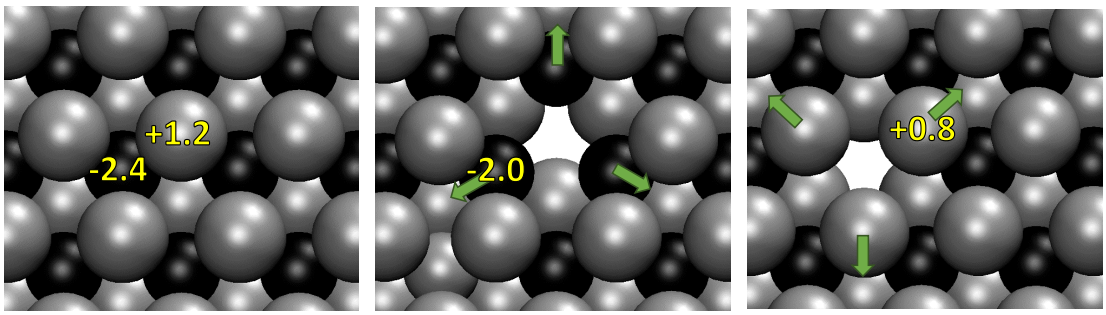

FIG. 3. Top views of the Ti_2C MXene when defect-free (left panel), with a Ti vacancy (center panel), or with a C vacancy (right panel), after relaxation of the positions of the atoms. Color code for spheres: C in black and Ti in grey. The numbers on the spheres are the calculated charges on the respective atoms, in electron charge units, and the green arrows point in the direction in which the associated atoms moved when the defect was created.

corresponding to V_C in Fig. 1 would maintain its shape but would be shifted upwards or downwards. On the other hand, the formation energy values of vacancies of the same kind on different surfaces can be directly compared. For instance, V_C are more likely to form on Mo_2C than on Ti_2C.

Calculation of the M-C bond orders (using the DDEC6 method described in Ref. [37]) yields similarly strong bonds for all the M_2C systems, between 0.83 and 0.91. This explains why, on group 4 and 5 MXenes, the formation energies range within 1 eV of each other. However, this does not explain the different behavior of the group 4 and 5 MXenes, compared to the group 6 ones. Instead, the way the MXenes are grouped suggests that the different behavior can be attributed to the metastability of the group 6 MXenes in their ABC atomic layer stacking configuration. In fact, since in this section we assume ABC stacking for all MXenes, despite group 6 MXenes being energetically more stable with ABA stacking, it stands to reason that structural defects are more easily formed on these MXenes—the symmetry breaking allows the lattice to undergo some reconstruction as an attempt to shift to ABA stacking. This can also be thought of in the other way around: more stable systems, such as the group 4 and 5 M_2C MXenes, require more energy to be broken. These two groups of MXenes also display distinct qualitative structural relaxation due to the presence of the defect, as well as distinct reconstruction energies (shown in Fig. S2 of the Supplemental Material [24]). The reconstruction energies of the V_M and V_C defects on M_2C MXenes of groups 4 and 5 are very small, around -0.1 eV for V_C and -0.4 eV for V_M. The surface relaxation due to the vacancies consisted of the neighboring atoms (C or M for V_M and V_C, respectively) moving around 0.1 Å away from the defect (see Fig. 3). In the case of V_M, this is a consequence of the fact that the C atoms are negatively charged and held in position by the positively charged M atoms—the removal of one M atom allows the nearby C ones to move away from the vacancy, towards other metallic atoms. For V_C, the same effect is observed, with the roles of C and M reversed. A Bader charge analysis also revealed that the three C atoms nearest to V_M became more neutral by around $0.3e$, while the six M atoms surrounding V_C become more neutral by around $0.4e$ on average. The Bader charge of the atoms closest to the vacancies on Ti_2C are shown in Fig. 3. On group 6 M_2C MXenes, we see a rather different picture when compared to those of groups 4 and 5. The reconstruction energies are 2 to 10 times as large (up to around -1 eV) and the motion of the atoms surrounding the defect occurs in the opposite direction (i.e., against the green arrows of Fig. 3). The former, along with the lower formation energy values, is likely due to the metastability of the ABC stacking on group 6 MXenes, and the latter can again be justified by an atomic charge argument. While the M and C atoms in groups 4 or 5 M_2C MXenes have charges of 1 to 3 electron charge units (as in the example of Ti_2C shown in Fig. 3), on group 6 ones, the atoms of the surface are much more neutral, with the M atoms having charges of less than $+0.8e$, and the C atoms less than $-1.6e$. The removal of a single atom from the lattice causes the nearby atoms to become even more neutral and allows them to come closer to each other, approaching their neutral covalent bond length. This is especially noticeable in the relaxation of the M atoms surrounding a V_C; for instance, on Mo_2C, the Mo-Mo distance of the Mo atoms closest to the defect is shortened by 0.27 Å after surface reoptimization. In some sense, the C atoms occupy a much smaller volume on group 6 MXenes than on groups 4 and 5 ones. For example, the calculated Bader volumes of a C atom on Ti_2C and V_2C are 26 and 18 $Å^3$, respectively, while on Mo_2C and W_2C they are 10 and 9 $Å^3$, respectively.

Let us now turn our attention to M_2N MXenes. Energetically, all V_M defects are easier to form than on their M_2C counterparts. This is likely due to the intrinsically weaker M-N bonds, compared with the corresponding M-C bonds [38]. For instance, the Ti-C and Ti-N bond orders in the Ti_2C and Ti_2N MXenes, calculated using the method of Manz *et al.* [37], are 0.83 and 0.73, respectively. All the calculated M-N bond orders are smaller than 0.84, and gradually decrease along the right-hand plot in Fig. 1, up to 0.60 on W_2N. Within our consideration that the energy of one N atom is half that of N_2, the X vacancies appear to be much harder to form on group 4 MXenes, with V_N having formation energies at least 2.5 eV higher than V_M. The V_N formation energies on Mo_2N and W_2N appear to be negative. This also stems from our assumption that the energy of one N atom is half that of an N_2 molecule. Thus, a negative formation energy means that the whole system is thermodynamically more stable when the N atom is bonded to another N atom, to form gaseous N_2, than when it is included in the MXene surface. The general trend is that both V_M and V_N formation energies decrease along each group or period of the Periodic Table, which may be a

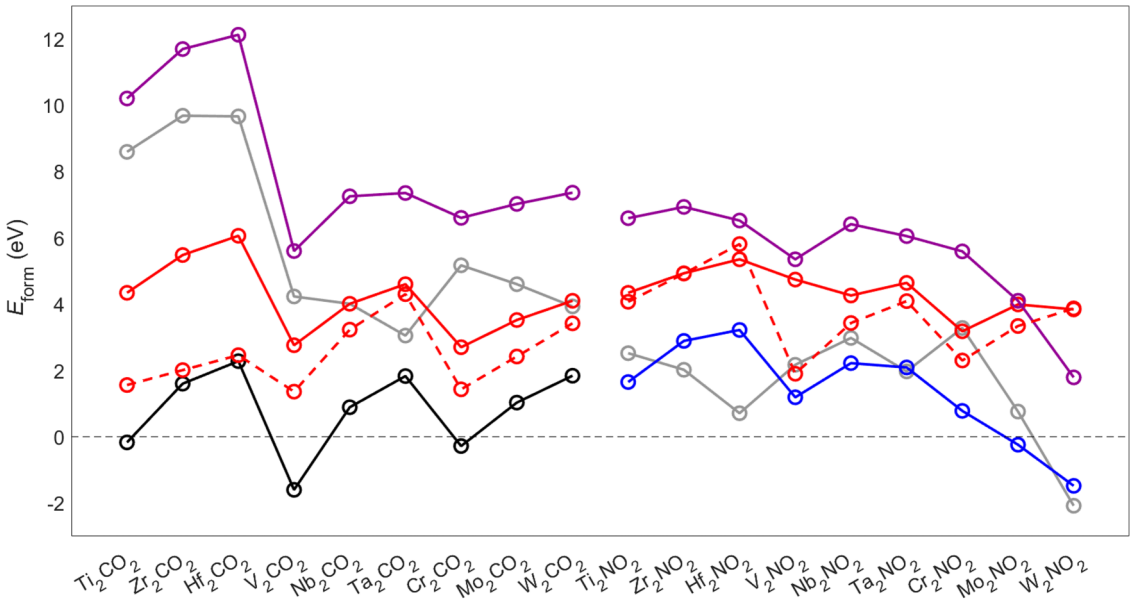

FIG. 4. Formation energies of vacancies in M_2XO_2 MXenes (values taken from Table S3 [24]). Carbides are shown on the left side, and nitrides on the right. The grey lines denote metal vacancies, the black and blue lines denote carbon or nitrogen vacancies, respectively, the full red lines denote oxygen vacancies, and the purple lines correspond to metal-oxygen double vacancies. The dashed red lines correspond to the formation energy of an oxygen vacancy neighboring a metal vacancy. The dashed grey line is placed at $E_{form} = 0$. Note that different reference species were considered in the calculation of E_{form} for different types of vacancies and direct comparison must consider this premise.

consequence of the M-N bond orders, which follow the same tendency. As the V_N curve is steeper than the V_M one (most likely due to each N atom being bonded to six other atoms while the M atoms only form three bonds) the former eventually dives under the latter, coincidentally near the zero-energy line. The reconstruction energies and relaxed structures of V_M and V_N on group 4 and 6 MXenes follow the same pattern as on the corresponding M_2C surfaces. However, group 5 M_2N MXenes display E_{form} values between those of M_2N MXenes of groups 4 and 6, contrasting with the M_2C case, in which group 5 surfaces behave as group 4 ones. This may be related to their shift in stacking preference, from ABC to ABA [7]. In fact, and as one might expect, the values in Fig. 2 suggest that the M_2X MXenes which prefer an ABA layer stacking, or for which the two possible layer alignments are almost equally stable, are more prone to contain defects in their ABC configuration.

B. Oxygen-terminated MXenes

We now focus on MXene surfaces terminated by an O layer, which becomes the preferential termination for MXenes after washing (F terminations are rinsed) and exposure to high-temperature treatment (surface OH groups yield the terminating oxo species). With this termination, the preference of MXenes for ABC or ABA stacking is maintained relatively to the pristine surfaces, but the results presented in this section are for ABC only. On the studied M_2CO_2 surfaces made of metals of groups 4 or 5, the O layer atoms are aligned with those of the farthest M layer, as seen in the leftmost panel of Fig. 1, while on group 6 MXenes, the O atoms align with the C layer atoms. This yields an overall O-M-C-M-O layer stacking of CABCA for group 4/5 M_2CO_2 MXenes, and BABCB for group 6 ones. The nitride MXenes of groups 4 and 6, and V_2NO_2, retain the O layer adsorption site from their carbide counterparts, while Nb_2NO_2 and Ta_2NO_2 shift their favored O layer alignment to that of the group 6 MXenes, i.e., the O atoms align with the N layer.

For M_2XO_2 MXenes, we considered four kinds of vacancy defects: M and X vacancies, as in the case of M_2X MXenes, O vacancies, and MO double vacancies, which have been observed in MXenes and can act as anchoring sites for single-atom catalysis [23]. The calculated vacancy formation energy values are plotted in Fig. 4, and the respective values are disclosed in Supplemental Material Table S3 [24].

On M_2CO_2 surfaces, V_M generally present the highest formation energies among all the single vacancies, followed by V_O, while V_C appear to be the most likely to be found on any of the M_2CO_2 MXenes studied. Although this ordering agrees with the literature on vacancy defects on M_2XO_2 MXenes [21], one must always keep in mind that formation energy values depend on the species that are considered as reference. Furthermore, like in other studies of vacancy formation on MXenes [21,22], here we only consider the thermodynamics of the system, i.e., we only compare the state of the system before and after the atom is removed, not accounting for energy barriers that need to be surmounted in the process. This is likely to be especially relevant in the case of vacancies in the innermost layer of the MXene, V_X, whose formation involves the motion of many atoms. The formation energies of all single and double vacancies tend to increase as a function of M along each group of the Periodic Table, indicating stronger bonds. Structurally, the creation of V_M defects involves breaking six bonds: three M-C and three M-O. The latter are especially strong due to the oxophilicity of MXenes.

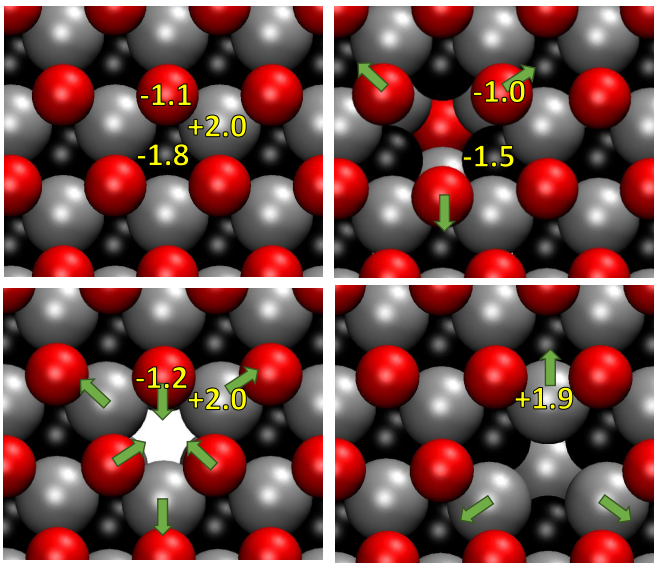

FIG. 5. Top views of the Ti_2CO_2 MXene when defect-free (top left panel), with a Ti vacancy (top right panel), with a C vacancy (bottom left panel), or with an O vacancy (bottom right panel), after relaxation of the positions of the atoms. Color code for spheres: C in black, Ti in grey, and O in red. The numbers on the spheres are the calculated charges on the respective atoms, in electron charge units, and the green arrows point in the direction in which the associated atoms moved when the defect was created.

This justifies the extremely high formation energy values of V_M on M_2CO_2, when compared to those on the corresponding M_2C. This is in line with experimental results on the thicker $Ti_3C_2T_x$ MXene. Ti vacancies have been observed experimentally on this material [39], and predicted to be much harder to form when the surface is covered by O than when it is bare [40].

The surface relaxation of the M_2CO_2 MXenes due to V_M consists mainly of the nearby O atoms being pushed away from the defect center, as in the example of Ti_2CO_2 shown in Fig. 5. The other two single-atom defects, V_C and V_O, cause the nearest M atoms to move away from the defect, repelled by the positive charge of each other. The creation of C vacancies additionally pulls in the surrounding O because both C and O are negatively charged. The way the lattice reconstructs around the vacancy can be justified by the conjugation of two effects. The first is an electric charge argument: the removal of an atom with a certain charge attracts surrounding atoms with like charges and repels nearby atoms with the opposite charge, as in Fig. 5. Second, when an atom becomes bonded to a smaller number of atoms (because one of them was removed), each of the remaining bonds becomes stronger, and naturally shorter. These effects are most evident in the relaxation due to V_M, which leads the three surrounding O adatoms to move away from each other, because of lateral Coulomb repulsion due to their negative charges, which was already present in the defect-free material, and the fact that one of the M-O bonds has disappeared, strengthening the remaining two. In the example of Ti_2CO_2, the length of the Ti-O bond formed by the three adjacent O adatoms is reduced by 7%, from 1.97 to 1.83 Å, accompanied by an increase of almost 50% in bond order, from 0.43 to 0.64. The relaxation due to V_{MO} is simply a superposition of the ones of V_M and V_O, along with V_{MO} formation energies rather well correlated with the sum of the formation energies of V_M and V_O (see Fig. S5 [24]), with a linear correlation coefficient of $R^2 \approx 0.96$. This analysis includes both carbide and nitride MXenes, as they were found to fit the same linear regression line.

The absolute values of the reconstruction energies due to V_M and V_C defects on M_2CO_2 MXenes are significantly higher than on the corresponding M_2C. While on the latter, these energies were of the order of -0.1 to -0.4 eV, the former present reconstruction energies of several eV, as shown in Fig. S4. The reconstruction energy of -1.78 eV calculated for V_M on Ti_2CO_2 agrees with the value -1.60 eV calculated in Ref. [21]. The small variation may be due to the slightly different computational and structural parameters considered in this work and in Ref. [21]. For V_C on Ti_2CO_2, we calculated a reconstruction energy of -1.38 eV (again agreeing with the -1.27 eV in Ref. [21]). The remaining M_2CO_2 MXenes have V_C and V_O reconstruction energies between -0.1 and -2.1 eV, and between -0.1 and -0.7 eV, respectively. The very low V_O reconstruction energies were expected since, although MXenes are very oxophilic, the T layer (O in this case) is not essential for their structural stability. Thus, the integrity of the lattice does not suffer too much stress when part of the termination is removed.

Concerning M_2NO_2 MXenes, the observation of the right side of Fig. 4 shows a rather different picture than what is observed for M_2CO_2 concerning V_M formation energies, which are reduced with respect to the M_2CO_2 case by several eV, while those of V_O are around the same magnitude as in M_2CO_2. The reduction of V_M formation energies has two complementary explanations, coinciding with those given for the particular case of Ti_2CO_2 and Ti_2NO_2, studied in Ref. [21]. First, M-N bonds are intrinsically weaker than M-C ones, which is reflected in lower V_M formation energies on MXene nitrides than on carbides, throughout the whole paper. Second, as seen in the plots of Fig. 4, some M_2NO_2 MXenes display very negative V_M reconstruction energies, to a greater extent than the corresponding M_2CO_2. In particular, those of group 4 nitrides are over -3 eV and imply that the MXene is able to gain considerable stability when one of its M atoms is removed. The near independence between V_O formation energy values and the X element is likely a consequence of there being no direct bond between the X and O atoms. The surface relaxation due to the vacancies consists mostly of the surrounding atoms moving away from the vacant site, an effect which is again most noticeable in the motion of O atoms due to V_M and reflects in higher reconstruction energy absolute values associated to this defect. The O atoms are the ones whose position is affected the most when near a V_M, because it causes them to be bonded to only 2 neighbors, conferring them extra mobility. The reconstruction energies due to V_M are at least -1 eV, up to roughly -4.5 eV on V_2NO_2, an MXene whose ABC-stacked lattice is especially deformed in the presence of vacancies. The obtained V_M and V_N reconstruction energies on Ti_2NO_2 are -3.3 and -1.20 eV, respectively, in agreement with the corresponding values of -3.03 and -1.27 eV found in the literature [21]. The V_O reconstruction energies are generally very small, between

−0.6 eV on the group 4 M_2NO_2 MXenes and less than −0.1 eV on some group 6 MXenes.

As happened in the cases of the bare M_2X MXenes (Sec. III A), the great reduction of V_M formation energies, when moving from M_2CO_2 to M_2NO_2 surfaces, causes M vacancies to appear thermodynamically easier to create than N ones on nearly half of the M_2NO_2 surfaces. One can take advantage of this to implant single-atom catalysts that fill M vacancies, as demonstrated, e.g., in Ref. [18] for Pt SAC substituting Ti in the Ti_3C_2 MXene. In the specific case of Ti_2XO_2, when moving from X = C to X = N, the V_M formation energy is lowered by 6 eV, while that of V_X increases by 1.8 eV. This is still not enough to reverse the order of the formation energies, but they differ by less than 1 eV when X = N, down from almost 9 eV when X = C, in agreement with the predictions of Ref. [21]. The V_{MO} formation energies of M_2NO_2 MXenes correlate rather well with the sum of V_M and V_O, and interestingly fit the same regression line of M_2CO_2 MXenes.

Let us briefly discuss the electronic properties of some of these defects, namely the changes in the band gap of the material due to their presence. To this end, we employed the HSE06 hybrid exchange-correlation functional, since local and semilocal exchange-correlation functionals (such as the PBE functional employed in this work) are known to severely underestimate semiconductor band gaps. Most times, hybrid density functional theory (DFT) calculations result in similar structural and energetic properties as semilocal-DFT ones, but considerably different electronic properties, namely wider semiconductor band gaps. Predictions by hybrid functionals are almost always in better agreement with experimental results, at the cost of increasing computation times by several orders of magnitude, especially in plane-wave calculations (see, for instance, Ref. [41]). In the case of the semiconductor/metal character of pristine MXenes, there appears to be a qualitative agreement between results obtained using the PBE and the hybrid HSE06 functionals (as mentioned, for example, in a recent review [42]), even though, as expected, the latter predicts band gaps higher by more than 1 eV in some cases. As for defective MXenes, results were obtained using the PBE functional for Ti_2CO_2 and Ti_2NO_2 [21], and for Ti_2CO_2 only [22]. In these references, the pristine Ti_2CO_2 MXene is predicted to be a semiconductor with a band gap around 0.26 eV, and to become a metal upon introduction of any kind of single-atom vacancy. The first of these two references additionally predicts Ti_2NO_2 to undergo the opposite, metal-to-semiconductor transition when a Ti or O vacancy is introduced, opening up an energy band gap below 0.1 eV. In our work, we found results similar to those of these two references.

Our single-point calculations using HSE06, performed on the Ti_2CO_2, Ti_2NO_2, V_2CO_2, and Cr_2CO_2 structures obtained with the PBE functional, yielded formation energies within 0.2 eV of the ones found using PBE. The V_2CO_2 surface was predicted to be metallic by our PBE (agreeing with Ref. [43]) and HSE06 calculations, both when pristine and when containing a V vacancy. In the presence of a V_C or V_O, the material is metallic if the PBE functional is used, but has a band gap of approximately 0.16 eV with HSE06. For Cr_2CO_2, both crystalline and with a single-atom vacancy, our calculations using either PBE or HSE06 resulted in small negative indirect band gaps, i.e., semimetallic behavior, in agreement with the results in Ref. [44]. On the Ti_2XO_2 MXenes, our HSE06 calculations resulted in a pristine Ti_2CO_2 band gap of 1.13 eV (in agreement with the one found in the literature [45,46]). The introduction of a V_C caused a semiconductor-to-metal transition, while V_O and V_{Ti} reduced the band gap to 0.16 and 0.27 eV, respectively, contrasting with PBE, which predicts no band gap at all for any single-atom vacancy. Concerning Ti_2NO_2, our calculations using PBE agree with the literature [21] in that they also indicate that the defect-free MXene is metallic, and a single-atom vacancy opens a very small band gap (around 0.1 eV or less). With HSE06, the pristine surface also appears metallic and adding an N or O vacancy creates an energy gap like the one predicted by the PBE functional. However, the Ti vacancy opens up a larger gap, around 0.60 eV. From these examples, we conclude that, although the PBE functional predicts the same qualitative results as HSE06 for pristine MXenes, it may incorrectly (compared to HSE06) predict the metallicity of some defective MXenes. The energy gaps predicted using HSE06 are all greater than or equal to the ones obtained using PBE but, at least in these examples, are small enough that charged defect levels are unlikely to be found within the band gap. In order to be certain, one would have to calculate the formation energies of charged defects and compare them with the formation energies of the corresponding neutral defects, for Fermi energies spanning the band gap, preferably using a hybrid functional for all calculations, which is beyond the scope of this work. Note that our hybrid-DFT calculations were worked out on geometries obtained using the PBE functional, so that a more comprehensive analysis should further optimize the atomic models using HSE06.

From observation of the lines corresponding to MO vacancy formation energies in Fig. 4, it appears that the creation of these defects is unfeasible. However, the formation of these divacancies can be facilitated by the HF (aq) etching procedure. In fact, Zhao *et al.* mention that some Ti atoms adjacent to the exfoliated Al layer are also etched off even under mild conditions when synthesizing the $Ti_3C_2T_x$ MXene [18]. In such cases, terminating O atoms in the vicinity of the Ti vacancy become bound to two instead of three Ti atoms and, therefore, the removal of the O atom often becomes easier (shown by the dashed red line in Fig. 4). Note that the introduction of the Ti vacancy reduces the number of bonds formed by the surrounding O adatoms, but this in turn strengthens the bonds that do remain. If the latter effect is dominant, the O adatoms may turn out to be more tightly bound to the surface, as predicted for Hf_2NO_2. Our calculations hint towards a formation energy reduction from 4.34 to 1.56 eV, for removing an O atom in a perfect Ti_2CO_2 model, versus in a Ti_2CO_2 slab with a neighboring Ti vacancy, respectively. Formation energy reductions of several eV can also be observed on many of the other MXenes, especially on the carbide MXenes with metals of group 4 of the Periodic Table. This also suggests that postsynthesis processes which remove the oxygen termination may in fact create MO vacancies, since O adatoms neighboring M vacancies should be the first ones to get removed. The occurrence of these MO vacancies was in fact observed in the $Mo_2TiC_2T_x$ MXene [23]. An alternative means to produce

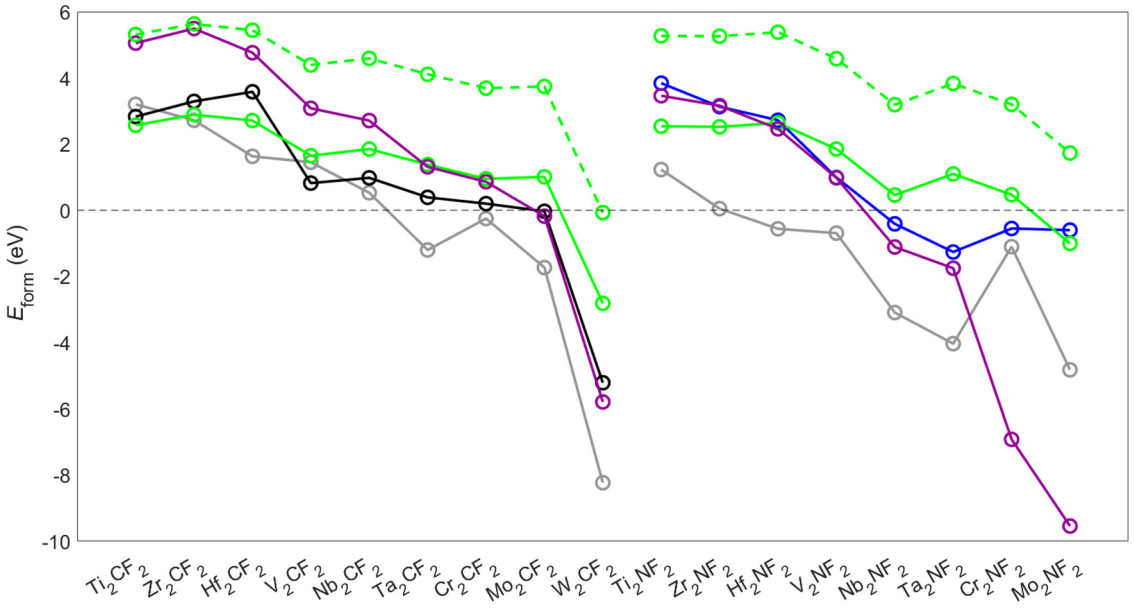

FIG. 6. Formation energies of vacancies in M_2XF_2 MXenes (values taken from Table S6). Carbides are shown on the left side, and nitrides on the right. Data for W_2NF_2 are shown in Table S6 but omitted here to allow a clearer visualization of the other points. The grey lines denote metal vacancies, the black and blue lines denote carbon or nitrogen vacancies, respectively, the full green lines denote fluorine vacancies, and the purple lines correspond to metal-fluorine double vacancies. The dashed green lines correspond to the formation energy of a fluorine vacancy, assuming the energy of a fluorine atom is $E(F_2)/2$. The dashed grey line is placed at $E_{form} = 0$. Note that different reference species were considered in the calculation of E_{form} for different types of vacancies and direct comparison must consider this premise.

MO vacancies is suggested by the fact that, in 16 of the 18 MXenes present in Fig. 4, the V_{MO} formation energy is lower than the sum of the $E_{form}(V_M) + E_{form}(V_O)$, most notably in Ti_2CO_2, Zr_2CO_2, and Hf_2CO_2, where the difference surpasses 2.7 eV. This indicates that V_M and V_O are attracted to each other. The attraction makes sense from the electrostatic point of view, since these two types of vacancies are surrounded by atoms with charges of opposite signs. Thus, the formation of an MO vacancy may not occur directly via the removal of two atoms simultaneously, but through the combination of a V_M and a V_O. To verify this possibility, we investigated the mobility of these two defects on Ti_2CO_2 using the dimer method [47]. We found that the migration barrier of an O vacancy on this MXene surface is 1.40 eV, which is much lower than its formation energy of 4.34 eV. Therefore, the vacancy can easily move along the lattice, potentially combining with a Ti vacancy to form a V_{TiO}. The migration barrier of V_{Ti} was calculated at 2.18 eV, a value higher than that of V_O, but still much lower than the V_{Ti} formation energy of 8.59 eV.

C. Fluorine-terminated MXenes

The lattice site on which the F termination sits depends on the M and X elements. On carbide MXenes, the F layer adsorbs on hollow sites with an M atom underneath, as in the left panel of Fig. 1. On the nitrides, the F termination lies on the same position as on carbides on all MXenes except Hf_2NF_2, Ta_2NF_2, and Cr_2NF_2, for which the F layer is aligned with the N one. The calculated formation energies of vacancies in fluorine-terminated MXenes (M_2XF_2) are shown in Fig. 6 and Table S6 [24].

The formation energy of any vacancy on M_2XF_2 MXenes decreases as a function of the M element along each group and period of the Periodic Table. On nearly all M_2XF_2 MXenes, V_M seems to be the defect most likely to occur. This ease of creating M vacancies was also observed in the previous section on nearly half the M_2NO_2 MXenes and, again, is especially relevant for catalytic applications that involve doping the surface with substitutional metallic atoms. By comparing Figs. 4 and 6, it becomes clear that V_M are much easier to create, by 6 eV on average, on M_2CF_2 MXenes than on M_2CO_2 ones. For example, a Ti vacancy in Ti_2CF_2 displays a formation energy lower by 5.39 eV than on Ti_2CO_2. The same difference was calculated at 5.17 eV in Ref. [21]. This is likely a consequence of M-F bonds generally being weaker than M-O ones. Experimentally, V_{Ti} formation energies have been obtained for Ti_3C_2, Ti_3C_2F, and Ti_3C_2O, the latter being more than twice as high as the former two, which in turn have similar values [40]. As for V_X and V_T, the changes in the formation energies are generally milder, up to 3 eV, except on W_2XT_2. Considering again the example of Ti_2CT_2, changing the termination from T = O to T = F, the V_C and V_T formation energies change by 3.00 and −1.77 eV, respectively. The first of these values is in agreement with the corresponding one (2.90 eV) in Ref. [21], but the difference between the formation energies of V_F in Ti_2CF_2 and V_O in Ti_2CO_2 calculated in Ref. [21] is positive, 0.65 eV. We found that this is simply due to the difference in the method of calculation of the energy of a fluorine atom. If we assume that the energy of an F atom is $E(F_2)/2$, we find higher formation energy values for V_F (dashed green line in Fig. 6). With this method, the difference between $E_{form}(V_F)$ and $E_{form}(V_O)$ in Ti_2CT_2 becomes 0.97 eV.

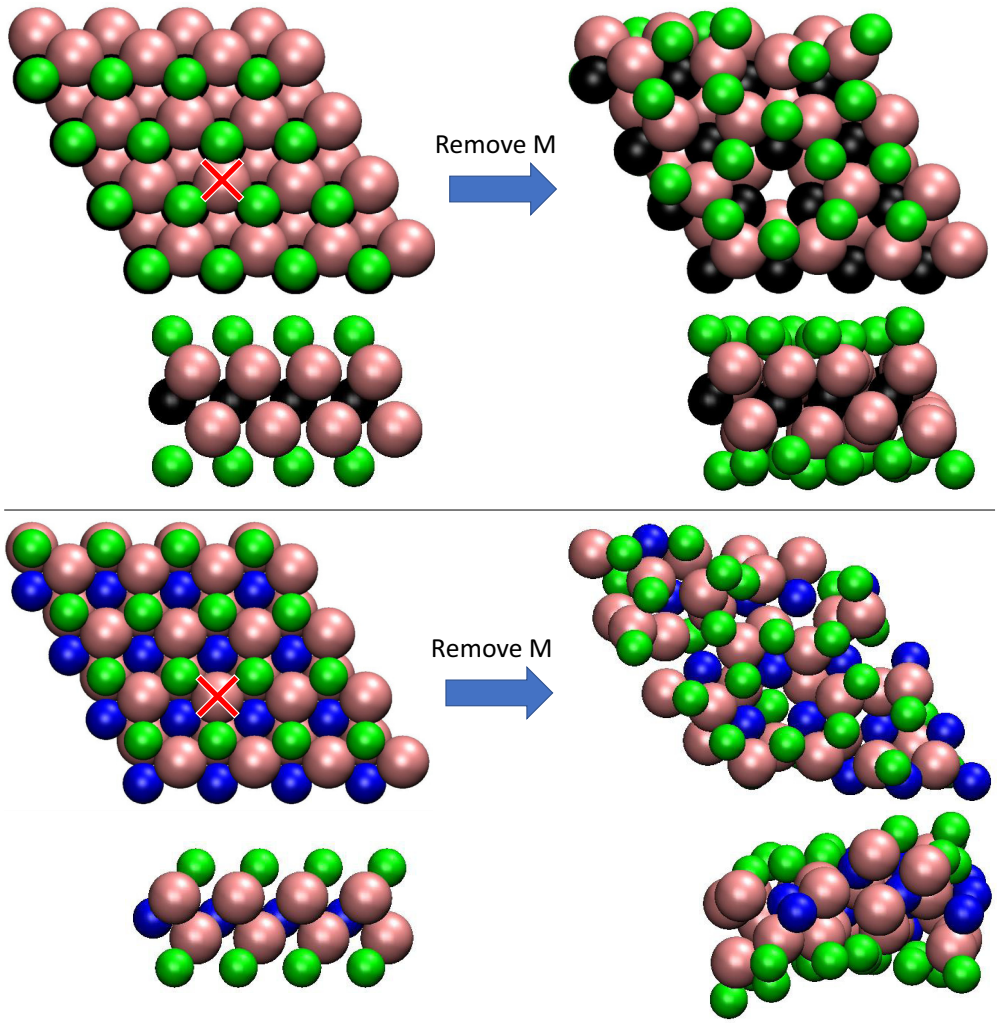

FIG. 7. W_2CF_2 (top diagrams) and W_2NF_2 (bottom diagrams) MXene surfaces, before (left) and after (right) the creation of a W vacancy, by removing the atom marked by the red cross on the left images. In each rectangle, the top and bottom schematics represent top and side views of the surface, respectively. Color code for spheres: C in black, N in blue, F in green, and W in pink.

Most of the vacancy defects on M_2XF_2 MXenes studied here induced only minor relaxation of the positions of the nearest atoms, similarly to the M_2XO_2 case. However, some of them caused major lattice deformation, namely on M_2NF_2 MXenes made of metals of group 6 of the Periodic Table, as well as on Mo_2CF_2, W_2CF_2, Nb_2NF_2, and Ta_2NF_2. All these cases are accompanied by very negative vacancy formation energy values, not because the corresponding atoms are easy to remove from the surface, but because of the lattice reconstruction that their absence allows (see Fig. S7). In these cases, the defect-free M_2XF_2 surfaces are metastable in the ABC atomic layer stacking configuration, in the sense that the atoms return to their original positions if they are slightly nudged in random directions, but this layer stacking is not the most stable energetically, as we will see in the next section. The most noticeable examples of the aforementioned lattice distortion are W_2CF_2 and W_2NF_2, shown in Fig. 7 for the most noteworthy case of V_M. The W vacancy in W_2NF_2 has the lowest vacancy formation energy (see Table S6), around -27 eV, with a concomitant damaging of its structural integrity. Due to the bizarre results of W_2NF_2, we repeated the relaxation of the atomic positions with the V_M defect, in a refined way, consisting of two tweaks. First, the motion of the atoms after each step was reduced to 1/5 of the default value. Second, instead of optimizing all atomic positions from the start, the lattice relaxation was partitioned: initially, only the atoms closer to the vacancy were moved to their new ground state positions, then the second-nearest neighbors, and finally all the atoms were allowed to move. The resulting configuration was again a disordered structure, and the sequence of reconstruction energies added up to around the same value as the one presented in Fig. S7 for V_M in W_2NF_2, thus confirming that the stability of this MXene is very sensitive to the presence of defects. Excluding the data relative to group 6 M_2NF_2 MXenes, V_{MF} formation energy values correlate reasonably well with the sum of the formation energies of V_M and V_F (Fig. S8), with a linear correlation coefficient of $R^2 \approx 0.97$.

D. Effect of the atomic layer stacking of MXenes

Some MXenes are understood to be energetically more stable when their M-X-M layers are stacked in an ABA fashion,

TABLE I. Energetic difference per formula unit, ΔE_{stack}, in eV, between ABA and ABC atomic layer stacking on the studied M_2XF_2 MXenes. Negative values in bold indicate preference towards ABA layer alignment.

Metal	X = C	X = N
Ti	1.04	0.76
Zr	1.40	0.62
Hf	1.62	0.53
V	0.18	0.21
Nb	0.18	**−0.05**
Ta	**−0.16**	**−0.21**
Cr	**−0.16**	**−0.67**
Mo	**−0.27**	**−0.51**
W	**−0.63**	**−1.03**

rather than the usual ABC one. This preference is known to be enhanced when (i) the M element is of a later group or period of the Periodic Table, (ii) the X element is N instead of C, and (iii) the MXenes are O terminated, rather than bare [7,35]. In this work, we found that some MXenes also prefer to display an ABA layer alignment when terminated by fluorine (see Table I). Resembling the O-terminated situation, the group 4 M_2XF_2 MXenes prefer ABC stacking, while group 6 ones prefer ABA stacking, with emphasis on W_2NF_2, exhibiting an energetic difference per formula unit of −1.03 eV. Concerning group 5 MXenes, the relative stability of both stackings depends on the M and X elements. In fact, the V-based and Ta-based M_2XF_2 MXenes prefer ABC and ABA, respectively, while the Nb_2XF_2 ones prefer ABC or seem to be equally stable with both possibilities, depending on whether the X element is C or N, respectively.

For half of the M/X MXene combinations—those of group 6 and the group 5 nitrides—we repeated the analysis of the previous sections, considering ABA layer stacking and bare, O-terminated, and F-terminated surfaces. We additionally recalculated the vacancy formation energies for all the group 5 M_2CF_2 MXenes, since they are also candidates to occur with an ABA layer alignment.

The calculated formation energy values for the bare MXenes with ABA stacking are shown in Fig. 8 and Table S9. All values in this table are higher than the corresponding ones on bare ABC-stacked MXenes (Fig. 2 and Table S1), and none of them is negative. The group 5 MNenes now follow the same trend as ABC-stacked group 4 ones, with V_M and V_N formation energies around 1.5 eV, and between 3 and 4 eV, respectively. The formation of V_X defects on bare group 6 MXenes is still noticeably easier than when M belongs to groups 4 or 5. This shows that the relatively low formation energies of V_X on group 6 MXenes, observed in both Figs. 2 and 7, are not only due to the layer alignment considered, but due to the M element itself. One of the reasons for the higher formation energies found when some MXenes are assumed to have an ABA layer is that, since the lattice may now be more stable, it does not reconstruct itself as much when a vacancy is present (full vs dashed lines in Fig. S2). For example, the reconstruction energy due to V_N is −1.16 eV on ABC W_2N, and it becomes only −0.16 eV when ABA stacking is considered instead.

Concerning O-terminated, ABA-stacked MXenes, the vacancy formation energies are displayed in Fig. 9 and Table S10. In this case, nearly all values are higher than the ones for ABC stacking (Fig. 4 and Table S3). The notable exception is V_O formation energies on nitrides, indicating that these ABA-stacked nitride MXenes are slightly less oxophilic than the respective ABC-stacked ones. Once again, this may be because a part of the vacancy formation energy values is due to the relaxation of the lattice atoms surrounding the defect. If the lattice is more stable with ABA stacking, it stands to

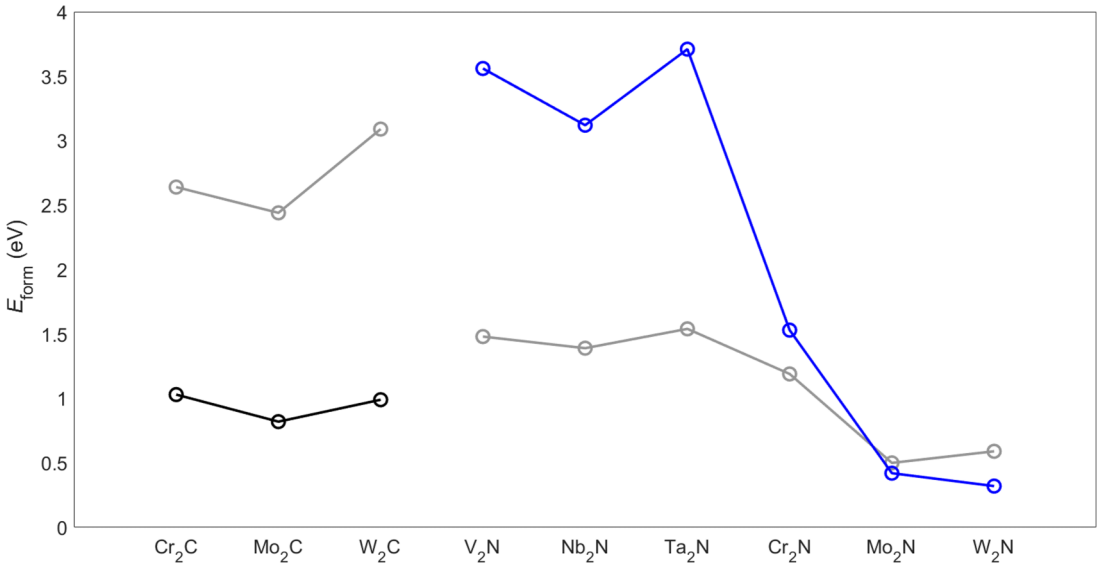

FIG. 8. Formation energies of vacancies in M_2X MXenes (values taken from Table S9) assuming ABA atomic layer alignment. Carbides are shown on the left side, and nitrides on the right. The grey lines denote metal vacancies, and the black and blue lines denote carbon or nitrogen vacancies, respectively. Note that different reference species were considered in the calculation of E_{form} for different types of vacancies and direct comparison must consider this premise.

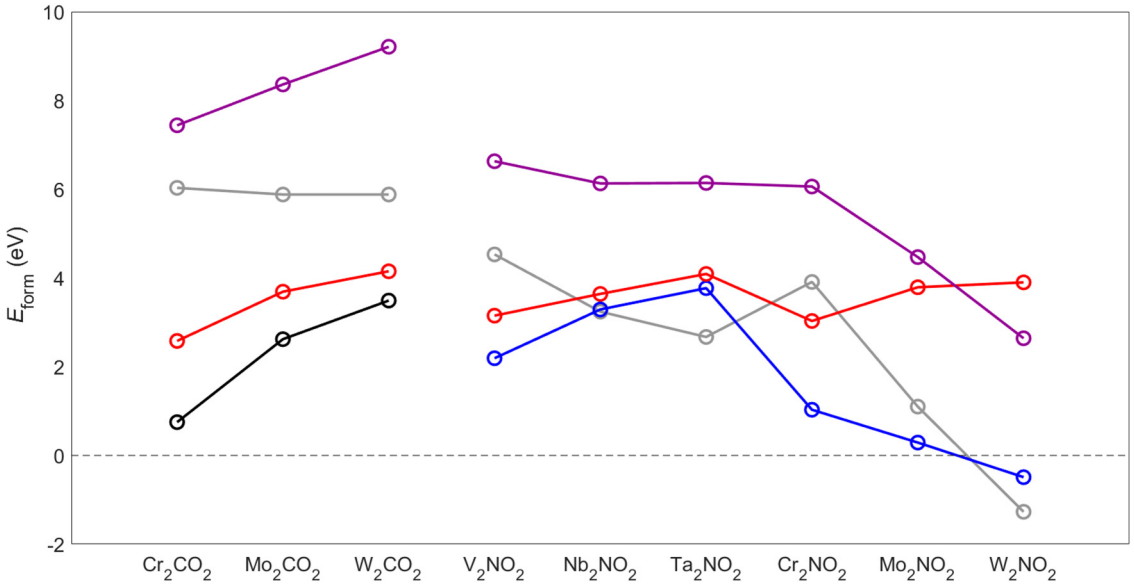

FIG. 9. Formation energies of vacancies in M_2XO_2 MXenes (values taken from Table S10) assuming ABA atomic layer alignment. Carbides are shown on the left side, and nitrides on the right. The grey lines denote metal vacancies, the black and blue lines denote carbon or nitrogen vacancies, respectively, the full red lines denote oxygen vacancies, and the purple lines correspond to metal-oxygen double vacancies. The dashed grey line is placed at $E_{form} = 0$. Note that different reference species were considered in the calculation of E_{form} for different types of vacancies and direct comparison must consider this premise.

reason that it will not undergo as much reconstruction when it is in the ABA phase. In line with the ABC results, on the ABA carbide MXenes, V_M appear to be the hardest single-atom defects to form, while V_C are the easiest, with formation energies differing by at least 2 eV, and increasing along the group of the periodic table of the M element. Also agreeing with the ABC data, some M_2NO_2 surfaces appear to be more likely to contain V_M than V_N defects. The linear correlation coefficient between V_{MO} formation energies and the sum of the formation energies of V_M and V_O is now $R^2 \approx 0.991$. When compared to bare ABA MXenes, the V_M formation energies on O-covered ABA MXenes are usually higher by several eV (as happened with the ABC structures, because the M atoms now form six bonds, as opposed to three on M_2X surfaces), the sole exception being W_2NO_2, on which removing an M atom costs nearly 2 eV less when in its ABA phase. In contrast, V_X become more or equally stable when the MXenes are terminated by O on most MXenes, but less stable by several eV on Mo_2CO_2 and W_2CO_2, as happened when assuming ABC layer alignment.

The calculated formation energy values for ABA-aligned M_2XF_2 MXenes are shown in Fig. 10 and Table S11. As expected, practically all values in this table are higher by several eV than the ones found for the same MXenes with ABC stacking (Fig. 6 and Table S6). The exceptions are V_F on V_2NF_2 and on Ta_2NF_2, whose formation energies become lower by 0.52 and 0.04 eV, respectively, when the stacking changes from ABC to ABA. These are the group 5 F-covered MXenes on which the ABC and ABA stackings display the highest relative stability, respectively. Importantly, and due to the preference for ABA stacking of some MXenes in Table I, there are no longer formation energy values of tens of eV. The lowest value is still attributed to V_M on W_2NF_2, but it is now -2.90 eV, higher than what is seen in Table S6 by more than 24 eV. The presence of this defect induced a reconstruction energy of around -1 eV and, like the other V_M defects in M_2NF_2 ABA MXenes, the lattice relaxation consists of the M atom under the vacancy being pulled towards the vacant site, attempting to fill it. Regarding the relative formation energies between the three types of single vacancies considered, V_M appear easier to create than V_X on all ABA-aligned MXenes, except for V_2CF_2, a fact that was observed with ABC stacking as well. As a matter of fact, M vacancies are the easiest to occur on nearly all M_2XF_2 MXenes, regardless of stacking. On this subject, another crucial difference between ABC and ABA stacking is that, on the former, V_X formation energies are lower than V_F ones, while they become higher than those of V_F on the latter. This may be another consequence of the higher stability of the ABA layer stacking, relatively to ABC, on most of these MXenes—if the MXene surface is more stable as a whole, it is harder to remove one of its essential atoms (M or X), and easier to remove its termination. As was predicted in all other cases throughout this study, here the formation energy of the MF double vacancy correlates approximately linearly with the sum of the formation energies of V_M and V_F, with $R^2 \approx 0.98$. In fact, R^2 becomes closest to 1 when the data of both M_2XO_2 and M_2XF_2 MXenes, with both ABC and ABA atomic layer stacking, are included in the fitting (Fig. S12). Remarkably, the corresponding fitted line allows the calculation of the formation energy of V_{MT} on MXenes made of any M, X, and T element combination, with either ABC or ABA atomic layer alignment, from the sum of the formation energies of V_M and V_T, with a mean absolute error of 0.36 eV.

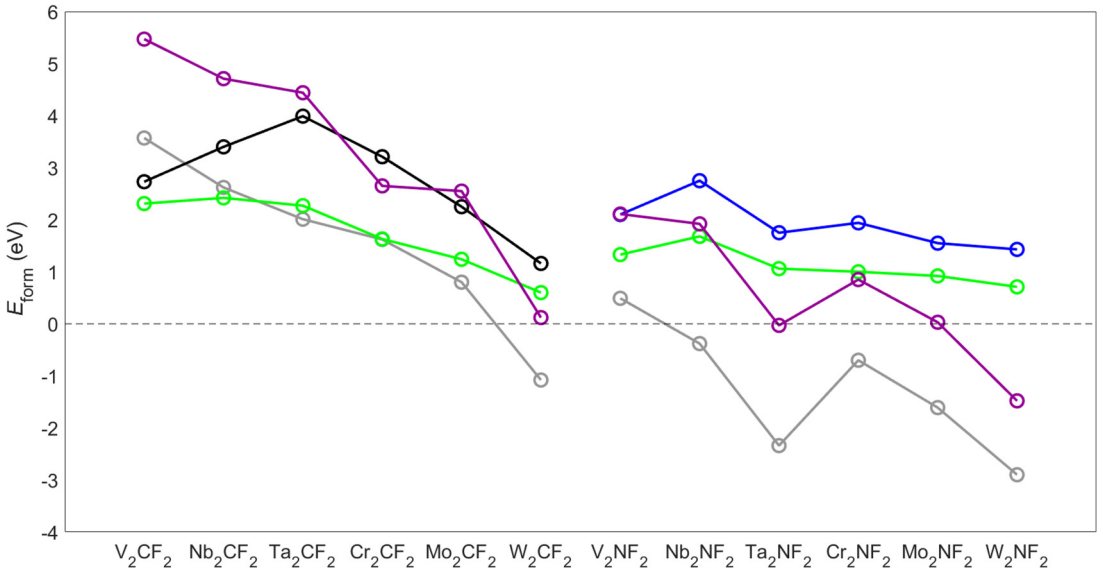

FIG. 10. Formation energies of vacancies in M_2XF_2 MXenes (values taken from Table S11) assuming ABA atomic layer alignment. Carbides are shown on the left side, and nitrides on the right. The grey lines denote metal vacancies, the black and blue lines denote carbon or nitrogen vacancies, respectively, the green lines denote fluorine vacancies, and the purple lines correspond to metal-fluorine double vacancies. The dashed grey line is placed at $E_{form} = 0$. Note that different reference species were considered in the calculation of E_{form} for different types of vacancies and direct comparison must consider this premise.

IV. CONCLUSIONS

In summary, we have analyzed the structure and energetics of vacancy defects on bare, O-terminated, and F-terminated MXene surfaces, both with ABC and ABA atomic layer stacking. Structurally, for the most part, the presence of the vacancy causes the atoms surrounding the vacant site to move away from the defect. This is because, on MXenes, consecutive atomic layers are oppositely charged. Therefore, the removal of one atom also removes the charge that was keeping the adjacent atoms closer together by screening their charge of the same sign. Without the missing charge, the nearby atoms are more strongly repelled by each other and move farther from the vacancy. This reconstruction energy was calculated at a few hundredths of eV in most cases.

We began by assuming ABC atomic layer stacking for all MXenes. On the clean carbide MXenes, we found that the formation energy of metal atom vacancies is approximately the same as that of carbon vacancies, usually between 2 and 3 eV. Changing the X element from C to N has the effect of reducing the metal vacancy formation energy while increasing that of the X vacancy, with the exceptions of Mo_2X and W_2X surfaces, on which metal vacancies are energetically more costly than C/N ones.

By covering the MXenes with a layer of O, the formation energies of metal atom vacancies were found to become considerably larger, reaching over 9 eV in some cases, while the X vacancy formation energies became smaller, with few exceptions. The F termination was found to decrease the formation energy of X vacancies as well, but to also decrease M vacancy formation energies, with respect to the bare MXenes. Comparing the O and F terminations with each other, we find that the F termination allows more easily created M and N vacancies, but leads to more unfavorable creation of C vacancies.

Some vacancies on ABC-stacked F-terminated MXenes displayed unrealistically low formation energies, such as that of the metal vacancy of W_2NF_2. This was found to be due to the metastability of these MXenes with this stacking. In fact, by creating a vacancy, one breaks the symmetry of the lattice and allows it to relax to a more stable form. In some cases, such as W_2NF_2, the resulting structure is a disordered amalgam of atoms, hardly recognizable as an MXene surface. For the cases in which ABA stacking is thermodynamically more stable or on par with ABC, i.e., MXenes made of metals of group 6 of the Periodic Table and most of the MXenes of group 5, we repeated the calculations considering ABA layer alignment. This had two major effects: first, lattice integrity was maintained; and second, the vacancy formation energies increased with respect to the ABC case. These two effects are connected because the vacancy formation energies include a surface reconstruction component. Since ABA stacking is favorable on most of the MXenes studied with this stacking, breaking the lattice symmetry by removing one atom did not induce as much surface relaxation as when ABC was assumed. In turn, less lattice reconstruction leads to higher formation energies, as the lattice was already stable before the vacancy was present.

By calculating the energy band gaps of the Ti_2CO_2, Ti_2NO_2, V_2CO_2, and Cr_2CO_2, pristine or with a single-atom vacancy, and comparing the results obtained using the PBE exchange-correlation density functional with those yielded by the HSE06 hybrid functional, we found a wide range of conducting behavior changes on these MXenes. Both functionals predict these materials to be semiconducting (Ti_2CO_2), metallic (Ti_2NO_2 and V_2CO_2), or semimetallic (Cr_2CO_2) when pristine. However, in the presence of a single-atom vacancy, the outcomes may differ depending on the functional used. For example, in agreement with results in the literature, we found

that the PBE functional predicts Ti_2CO_2 to become metallic upon introduction of any kind of single-atom vacancy, while HSE06 predicts a semiconducting behavior, with band gaps of 0.16 and 0.27 eV for V_O and V_{Ti}, respectively. This was to be expected, since PBE is known to underestimate the band gaps of semiconductors, an issue very commonly solved by employing a hybrid functional. Note that our hybrid-DFT calculations were performed on structures relaxed using the PBE functional, hence, for a more comprehensive analysis, one should fully optimize the atomic positions using HSE06.

Last, we found that the formation energies of the metal and termination double vacancies display an approximately linear correlation with the sum of the formation energies of the M and T single-atom vacancies. Remarkably, all MXene surfaces studied in this work, with all M, X, and T elements, and with both ABC and ABA atomic layer stackings, fit the same regression line. This allows one to predict the formation energy of double vacancies on any MXene surface, from the known formation energies of the corresponding single vacancies.

ACKNOWLEDGMENTS

This research was made within the scope of the project CICECO-Aveiro Institute of Materials, Grants No. UIDB/50011/2020, No. UIDP/50011/2020, and No. LA/P/0006/2020, financed by national funds through the Fundação para a Ciência e a Tecnologia (FCT/MEC, PIDDAC). We are also thankful to FCT I.P. for the computational resources granted in the framework of Project No. CPCA/A2/6817/2020 by the FCT/CPCA/2020/01 Call for Advanced Computing Projects. D.G. acknowledges project SILVIA Grants. No. CENTRO-01-0145-FEDER-31002 and No. PTDC/QUI-QFI/31002/2017.

[1] M. Naguib, V. N. Mochalin, M. W. Barsoum, and Y. Gogotsi, 25th Anniversary article: MXenes: A new family of two-dimensional materials, Adv. Mater. **26**, 992 (2014).

[2] M. Naguib, M. Kurtoglu, V. Presser, J. Lu, J. Niu, M. Heon, L. Hultman, Y. Gogotsi, and M. W. Barsoum, Two-dimensional nanocrystals produced by exfoliation of Ti_3AlC_2, Adv. Mater. **23**, 4248 (2011).

[3] T. Li, L. Yao, Q. Liu, J. Gu, R. Luo, J. Li, X. Yan, W. Wang, P. Liu, B. Chen, W. Zhang, W. Abbas, R. Naz, and D. Zhang, Fluorine-free synthesis of high-purity $Ti_3C_2T_x$ (T = OH, O) via alkali treatment, Angew. Chem. Int. Ed. **57**, 6115 (2018).

[4] I. Persson, J. Halim, H. Lind, T. W. Hansen, J. B. Wagner, L.-Å. Näslund, V. Darakchieva, J. Palisaitis, J. Rosen, and P. O. Å. Persson, 2D transition metal carbides (MXenes) for carbon capture, Adv. Mater. **31**, 1805472 (2019).

[5] E. B. Deeva, A. Kurlov, P. M. Abdala, D. Lebedev, S. M. Kim, C. P. Gordon, A. Tsoukalou, A. Fedorov, and C. R. Müller, *In situ* XANES/XRD study of the structural stability of two-dimensional molybdenum carbide Mo_2CT_x: Implications for the catalytic activity in the water–gas shift reaction, Chem. Mater. **31**, 4505 (2019).

[6] G. Deysher, C. E. Shuck, K. Hantanasirisakul, N. C. Frey, A. C. Foucher, K. Maleski, A. Sarycheva, V. B. Shenoy, E. A. Stach, B. Anasori, and Y. Gogotsi, Synthesis of Mo_4VAlC_4 MAX phase and two-dimensional Mo_4VC_4 MXene with five atomic layers of transition metals, ACS Nano **14**, 204 (2020).

[7] J. D. Gouveia, F. Viñes, F. Illas, and J. R. B. Gomes, MXenes atomic layer stacking phase transitions and their chemical activity consequences, Phys. Rev. Mater. **4**, 054003 (2020).

[8] R. Thakur, A. VahidMohammadi, J. Moncada, W. R. Adams, M. Chi, B. Tatarchuk, M. Beidaghi, and C. A. Carrero, Insights into the thermal and chemical stability of multilayered V_2CT_x MXene, Nanoscale **11**, 10716 (2019).

[9] M. Seredych, C. E. Shuck, D. Pinto, M. Alhabeb, E. Precetti, G. Deysher, B. Anasori, N. Kurra, and Y. Gogotsi, High-temperature behavior and surface chemistry of carbide MXenes studied by thermal analysis, Chem. Mater. **31**, 3324 (2019).

[10] L. Zhang, W. Su, Y. Huang, H. Li, L. Fu, K. Song, X. Huang, J. Yu, and C.-T. Lin, *In Situ* high-pressure x-ray diffraction and raman spectroscopy study of $Ti_3C_2T_x$ MXene, Nanoscale Res. Lett. **13**, 343 (2018).

[11] J. Peng, X. Chen, W. J. Ong, X. Zhao, and N. Li, Surface and heterointerface engineering of 2D MXenes and their nanocomposites: insights into electro- and photocatalysis, Chem **5**, 18 (2019).

[12] Á. Morales-García, F. Calle-Vallejo, and F. Illas, MXenes: New horizons in catalysis, ACS Catal. **10**, 13487 (2020).

[13] J. D. Gouveia, Á. Morales-García, F. Viñes, J. R. B. Gomes, and F. Illas, Facile heterogeneously catalyzed nitrogen fixation by MXenes, ACS Catal. **10**, 5049 (2020).

[14] J. D. Gouveia, G. Novell-Leruth, F. Viñes, F. Illas, and J. R. B. Gomes, The Ti_2CO_2 MXene as a nucleobase 2D sensor: A first-principles study, Appl. Surf. Sci. **544**, 148946 (2021).

[15] J. D. Gouveia, G. Novell-Leruth, P. M. L. S. Reis, F. Viñes, F. Illas, and J. R. B. Gomes, First-principles calculations on the adsorption behavior of amino acids on a titanium carbide MXene, ACS Appl. Bio Mater. **3**, 5913 (2020).

[16] C. Chen, M. Boota, P. Urbankowski, B. Anasori, L. Miao, J. Jiang, and Y. Gogotsi, Effect of glycine functionalization of 2D titanium carbide (MXene) on charge storage, J. Mater. Chem. A **6**, 4617 (2018).

[17] B. Huang, N. Li, W.-J. Ong, and N. Zhou, Single atom-supported MXene: How single-atomic-site catalysts tune the high activity and selectivity of electrochemical nitrogen fixation, J. Mater. Chem. A **7**, 27620 (2019).

[18] D. Zhao, Z. Chen, W. Yang, S. Liu, X. Zhang, Y. Yu, W.-C. Cheong, L. Zheng, F. Ren, G. Ying, X. Cao, D. Wang, Q. Peng, G. Wang, and C. Chen, MXene (Ti_3C_2) vacancy-confined single-atom catalyst for efficient functionalization of CO_2, J. Am. Chem. Soc. **141**, 4086 (2019).

[19] X. Yang, Z. Lu, C. Cheng, Y. Wang, X. Zhang, Z. Yang, and W. Lu, Identification of efficient single-atom catalysts based on V_2CO_2 MXene by ab initio simulations, J. Phys. Chem. C **124**, 4090 (2020).

[20] Z. Deng, X. Zheng, M. Deng, L. Li, L. Jing, and Z. Wei, Catalytic activity of V_2CO_2 MXene supported transition metal

single atoms for oxygen reduction and hydrogen oxidation reactions: a density functional theory calculation study, Chin. J. Catal. **42**, 1659 (2021).

[21] A. Bandyopadhyay, D. Ghosh, and S. K. Pati, Effects of point defects on the magnetoelectronic structures of MXenes from first principles, Phys. Chem. Chem. Phys. **20**, 4012 (2018).

[22] L. Xiao-Hong, S. Xiang-Ying, and Z. Rui-Zhou, Effect of vacancies on the structural and electronic properties of Ti_2CO_2, RSC Adv. **9**, 27646 (2019).

[23] J. Zhang, Y. Zhao, X. Guo, C. Chen, C.-L. Dong, R.-S. Liu, C.-P. Han, Y. Li, Y. Gogotsi, and G. Wang, Single platinum atoms immobilized on an MXene as an efficient catalyst for the hydrogen evolution reaction, Nat. Catal. **1**, 985 (2018).

[24] See Supplemental Material at http://link.aps.org/supplemental/10.1103/PhysRevMaterials.6.024004 for additional information about formation energies of vacancies in bare and terminated MXenes and reconstruction energies due to the presence of surface defects in MXenes.

[25] G. Kresse and J. Hafner, Ab initio molecular dynamics for liquid metals, Phys. Rev. B **47**, 558 (1993).

[26] G. Kresse and J. Hafner, Ab initio molecular-dynamics simulation of the liquid-metal–amorphous-semiconductor transition in germanium, Phys. Rev. B **49**, 14251 (1994).

[27] G. Kresse and J. Furthmüller, Efficient iterative schemes for ab initio total-energy calculations using a plane-wave basis set, Phys. Rev. B **54**, 11169 (1996).

[28] G. Kresse and J. Furthmüller, Efficiency of ab-initio total energy calculations for metals and semiconductors using a plane-wave basis set, Comput. Mater. Sci. **6**, 15 (1996).

[29] J. P. Perdew, K. Burke, and M. Ernzerhof, Generalized Gradient Approximation Made Simple, Phys. Rev. Lett. **77**, 3865 (1996).

[30] P. E. Blöchl, Projector augmented-wave method, Phys. Rev. B **50**, 17953 (1994).

[31] L. Vinet and A. Zhedanov, A 'missing' family of classical orthogonal polynomials, J. Phys. A: Math. Theor. **44**, 085201 (2011).

[32] J. D. Gouveia, Á. Morales-García, F. Viñes, F. Illas, and J. R. B. Gomes, MXenes as promising catalysts for water dissociation, Appl. Catal. B: Environ. **260**, 118191 (2020).

[33] N. Zhang, Y. Hong, S. Yazdanparast, and M. Asle Zaeem, Superior structural, elastic and electronic properties of 2D titanium nitride MXenes over carbide MXenes: A comprehensive first principles study, 2D Mater. **5**, 045004 (2018).

[34] W. Sun, Y. Li, B. Wang, X. Jiang, M. I. Katsnelson, P. Korzhavyi, O. Eriksson, and I. Di Marco, A new 2D monolayer BiXene, M_2C (M = Mo, Tc, Os), Nanoscale **8**, 15753 (2016).

[35] M. Shao, Y. Shao, W. Chen, K. L. Ao, R. Tong, Q. Zhu, I. N. Chan, W. F. Ip, X. Shi, and H. Pan, Efficient nitrogen fixation to ammonia on MXenes, Phys. Chem. Chem. Phys. **20**, 14504 (2018).

[36] P. Urbankowski, B. Anasori, K. Hantanasirisakul, L. Yang, L. Zhang, B. Haines, S. J. May, S. J. L. Billinge, and Y. Gogotsi, 2D molybdenum and vanadium nitrides synthesized by ammoniation of 2D transition metal carbides (MXenes), Nanoscale **9**, 17722 (2017).

[37] T. A. Manz, Introducing DDEC6 atomic population analysis: Part 3. comprehensive method to compute bond orders, RSC Adv. **7**, 45552 (2017).

[38] J. Häglund, A. Fernández Guillermet, G. Grimvall, and M. Körling, Theory of bonding in transition-metal carbides and nitrides, Phys. Rev. B **48**, 11685 (1993).

[39] L. H. Karlsson, J. Birch, J. Halim, M. W. Barsoum, and P. O. Å. Persson, Atomically resolved structural and chemical investigation of single MXene sheets, Nano Lett. **15**, 4955 (2015).

[40] X. Sang, Y. Xie, M.-W. Lin, M. Alhabeb, K. L. Van Aken, Y. Gogotsi, P. R. C. Kent, K. Xiao, and R. R. Unocic, Atomic defects in monolayer titanium carbide ($Ti_3C_2T_x$) MXene, ACS Nano **10**, 9193 (2016).

[41] J. D. Gouveia and J. Coutinho, Can we rely on hybrid-DFT energies of solid-state problems with local-DFT geometries?, Electron. Struct. **1**, 015008 (2019).

[42] A. Champagne and J.-C. Charlier, Physical properties of 2D MXenes: From a theoretical perspective, J. Phys. Mater. **3**, 032006 (2021).

[43] M. Khazaei, M. Arai, T. Sasaki, C.-Y. Chung, N. S. Venkataramanan, M. Estili, Y. Sakka, and Y. Kawazoe, Novel electronic and magnetic properties of two-dimensional transition metal carbides and nitrides, Adv. Funct. Mater. **23**, 2185 (2013).

[44] H. Weng, A. Ranjbar, Y. Liang, Z. Song, M. Khazaei, S. Yunoki, M. Arai, Y. Kawazoe, Z. Fang, and X. Dai, Large-gap two-dimensional topological insulator in oxygen functionalized MXene, Phys. Rev. B **92**, 075436 (2015).

[45] S. A. Khan, B. Amin, L.-Y. Gan, and I. Ahmad, Strain engineering of electronic structures and photocatalytic responses of MXenes functionalized by oxygen, Phys. Chem. Chem. Phys. **19**, 14738 (2017).

[46] Z. Guo, J. Zhou, L. Zhu, and Z. Sun, MXene: A promising photocatalyst for water splitting, J. Mater. Chem. A **4**, 11446 (2016).

[47] G. Henkelman and H. Jónsson, A dimer method for finding saddle points on high dimensional potential surfaces using only first derivatives, J. Chem. Phys. **111**, 7010 (1999).